

Comparison of the spin-transfer torque mechanisms in a three-terminal spin-torque oscillator

Cite as: J. Appl. Phys. **124**, 043904 (2018); <https://doi.org/10.1063/1.5042092>
Submitted: 29 May 2018 . Accepted: 12 July 2018 . Published Online: 30 July 2018

Emilie Jué, William H. Rippard, and Matthew R. Pufall



View Online



Export Citation



CrossMark

ARTICLES YOU MAY BE INTERESTED IN

[Asymmetric and partial injection locking of a three-terminal spin-torque oscillator](#)
Applied Physics Letters **112**, 102403 (2018); <https://doi.org/10.1063/1.5019729>

[Recent advances in spin-orbit torques: Moving towards device applications](#)
Applied Physics Reviews **5**, 031107 (2018); <https://doi.org/10.1063/1.5041793>

[Perspective: Spintronic synapse for artificial neural network](#)
Journal of Applied Physics **124**, 151904 (2018); <https://doi.org/10.1063/1.5042317>

Lock-in Amplifiers
up to 600 MHz



Comparison of the spin-transfer torque mechanisms in a three-terminal spin-torque oscillator

Emilie Jué,^{1,2} William H. Rippard,¹ and Matthew R. Pufall¹

¹Quantum Electromagnetics Division, National Institute of Standards and Technology, Boulder, Colorado 80305, USA

²Department of Physics, University of Colorado, Boulder, Colorado 80309, USA

(Received 29 May 2018; accepted 12 July 2018; published online 30 July 2018)

We have studied magnetization dynamics in three-terminal spin-torque oscillators (STOs) and present a direct method to compare the efficiencies of exciting oscillations in STOs through two mechanisms of spin transfer torque: the spin filtering torque (SFT) and the spin-orbit torque (SOT). The devices are composed of spin-valves patterned on a Pt wire that can be excited by a SFT and/or a SOT, depending on the pathway of the DC current. By varying the device and wire size, we tune and compare the efficiencies of both mechanisms in terms of current and current density. To a first approximation, for sufficiently narrow Pt wires (compared to the dimension of the spin-valve), significantly more current is required to excite the devices with SFT than with SOT, whereas in terms of current density, the SFT is up to three times more efficient than the SOT in the system studied. We investigate the limits of this comparison using control samples where the spin-valve is replaced by a magnetic tunnel junction (MTJ) or where the Pt wire is replaced by a Cu wire. A three terminal STO made with a MTJ is the most appropriate device to compare the efficiencies of both spin transfer mechanisms in order to avoid additional spin transfer torque induced by current shunted through the magnetic pillar. *Published by AIP Publishing.* <https://doi.org/10.1063/1.5042092>

I. INTRODUCTION

The manipulation of magnetization by electric current via the spin transfer torque (STT) mechanism is one of the most active fields within spintronics due to its potential applications in memory and logic devices.^{1–3} This control is achieved through the transfer of angular momentum via a spin polarized current in a magnetic heterostructure, either through the mechanism of spin-filtering torque (SFT)^{4,5} or through the direct transfer of angular momentum from the crystal lattice through the spin-orbit interaction, namely, the mechanism of spin-orbit torque (SOT).^{6–8} Over the past several years, SOT has gained significant attention for the new possibilities it offers for three-terminal data storage applications.^{3,9} However, due to the strong dependence of the magnitudes of both effects on the details of growth conditions and the significantly different device geometries, the quantification and the comparison of the two torques' relative efficiencies remain an open question.

In this letter, we report on a method to directly compare the SFT and SOT damping-like torque efficiencies in a single device. We created three-terminal spin-torque oscillators (STOs) composed of spin-valves (SVs) patterned on Pt wires. The devices can be excited either by SFT or by SOT depending on whether the current is applied through the SV or through the Pt wire. By varying the dimensions of the SVs and the wire widths, we tune the SOT and SFT and compare their efficiencies utilizing two different methods. Under the hypothesis that the STT induced through the Pt wire is entirely due to the SOT mechanism, we show that, for the dimensions that we studied, the SOT can be twice as efficient as the SFT in terms of current, whereas in terms of current density, the efficiency of SFT is higher than of SOT. Finally,

to discuss the limits of our method, we build and measure three other devices as control samples consisting of three-terminal devices where the Pt wire is replaced by a Cu wire or where the SV is replaced by a magnetic tunnel junction (MTJ). To avoid additional spin transfer torque induced by current shunted through the magnetic pillar, a three-terminal STO made with a MTJ is the most appropriate device to compare the efficiencies of both spin transfer mechanisms.

II. DEVICES AND EXPERIMENTAL SETUP

A. Description of the devices

The devices studied consist of a magnetic multilayered nanopillar (SV or MTJ) on a Pt or a Cu wire (the latter from which no SOT is expected). We thus have four different systems: SV on a Pt wire (SV-Pt), SV on a Cu wire (SV-Cu), MTJ on a Pt wire (MTJ-Pt), and MTJ on a Cu wire (MTJ-Cu). The SV-Pt is used to compare the efficiency of the spin transfer of the SFT and the SOT, whereas the three latter systems are used as control samples to discuss the limits of the method. The two SV-based devices are patterned from an initial multilayer of Ta(2)/underlayer(7)/CoFe(0.45)/[Ni(t_{Ni})/CoFe(t_{CoFe})] \times 3/Cu(3.5)/CoFe(5)/Cu(3)/Ta(4), and the two MTJ-based devices are patterned from an initial multilayer of Ta(2)/underlayer(7)/CoFe(t_{CoFe})/[Ni(t_{Ni})/CoFe(t_{CoFe})] \times 3/AlOx(1)/CoFe(5)/IrMn(11)/Ta(4), where the thicknesses are given in nanometers in parentheses, the CoFe composition is Co₉₀Fe₁₀, and the underlayer consists of a Pt or a Cu layer. The thick CoFe layer on top of the nanopillar acts as a reference layer with an in-plane magnetization, and the CoFe/Ni multilayer is the free layer. The thicknesses t_{CoFe} and t_{Ni} (both varying between 0.29 and 0.41 nm) are chosen to

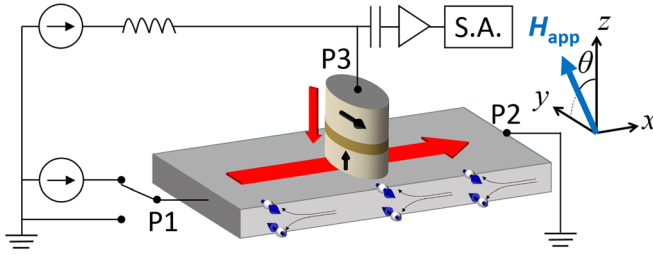


FIG. 1. Diagram of a three-terminal device consisting of a SV (or a MTJ) on a (or Cu) Pt wire. The device can be excited by SFT with a current through the magnetic pillar or by SOT with a current through the Pt wire (red arrows). Each current is applied with a different current source through a bias-tee from port P1 or P3 to the common ground at P2. The high-frequency power output is amplified and sent to the spectrum analyzer (S.A.). The magnetization of the reference layer is oriented along the y -direction in order to be aligned with the polarization of the spin-current induced in the Pt wire (blue arrows). The measurements are done in the presence of an external magnetic field H_{app} applied with a tilt angle θ from the z -axis.

adjust the perpendicular anisotropy,¹⁰ which is tuned to have the magnetization out-of-plane for the SV-based samples and in-plane for the MTJ-based samples. Finally, the devices are fabricated using two electron beam lithography (EBL) and argon-ion etching steps: the first step patterns the device into a wire with a width w_{Pt} or w_{Cu} varying from 300 nm to 700 nm and the second patterns the magnetic stack into an elliptical pillar up to the Pt or Cu underlayer. Endpoint detection of this etch is achieved via secondary ion mass spectrometry.

The results presented for the SV-Pt are obtained from two different wafers, denoted A and B. The sample from wafer A is composed of $50 \text{ nm} \times 150 \text{ nm}$ SV devices on a 400 nm wide Pt wire, and the sample from wafer B is composed of devices with different dimensions of SV ($50 \text{ nm} \times 150 \text{ nm}$ or $100 \text{ nm} \times 200 \text{ nm}$) and Pt widths (300 nm to 700 nm) in order to vary the current densities causing the SFT and the SOT. The length of the SOT line was adjusted to match its width in order to get similar values of resistances through the Pt wires for all devices. The SV-Cu system is built as a $50 \text{ nm} \times 150 \text{ nm}$ SV patterned on a 300 nm wide wire, and the two MTJ-based systems consist of a $50 \text{ nm} \times 150 \text{ nm}$ MTJ patterned on a 500 nm wide wire. The magnetic and electrical properties of each device are reported in Table I.

B. Experimental setup

The circuit used for the experiment is shown in Fig. 1. Considering the SV-Pt system, current passing through Pt is

used to exert an SOT on the free layer, whereas SFT is induced by passing current through the SV. Independent current sources are connected to ports P3 and P1, with a common ground at port P2. A switch on P1 is used to either connect the Pt wire to its current source or to ground both ends of the Pt wire, so that when the current is applied through the SV, it can flow into the Pt wire symmetrically [inset of Fig. 2(b)] or asymmetrically [inset of Fig. 2(b)]. The SV is oriented such that the reference layer's easy-axis is along the y -direction, such that the spin-polarization axis of the current through the SV is in the same direction as that of the spin-current induced by the damping-like torque of the SOT. The devices are current-biased, and a microwave precessional signal is measured with a spectrum analyzer via the giant magnetoresistance (GMR) effect when magnetization precession is induced in the device. All measurements are performed at room temperature in an external magnetic field oriented at an angle θ from the normal to the sample. The field angle is used to maintain the stability of the reference layer and improve the amplitude of the output signal.

III. MAGNETIZATION DYNAMICS AND METHODS

A. Influence of the current pathway on the magnetization dynamics

The physical STT mechanism (SFT or SOT) responsible for the STO excitation depends on the pathway of the DC current through the three-terminal device. Considering a SV-Pt system, we distinguish three different DC current excitations: (i) the current $I_{SV,Asym}$ flowing from P3 to P2 [inset of Fig. 2(a)], inducing an excitation of the device by SOT and SFT simultaneously; (ii) the current $I_{SV,Sym}$ flowing from P3 to P1 and P2 [inset of Fig. 2(b)], inducing an excitation of the device by only the SFT (because the SOT is, on average, cancelled with current flowing in both directions in Pt); and (iii) the current I_{Pt} flowing from P1 to P2 [inset of Fig. 2(c)], inducing an excitation of the device by the SOT only. The notations $I_{SV,Asym}$, $I_{SV,Sym}$, and I_{Pt} describe the three different current pathways.

Figure 2 shows STO excitations for a SV-Pt device (from wafer A) for the three different DC current excitations. All three excitation methods show a similar onset frequency, but a shift in the critical current for the onset of oscillations, and different slopes for frequency vs. current. When the current is applied through the SV, two cases have to be distinguished. For a current $I_{SV,Asym}$, the current flows through the SV and into one half of the Pt wire [Fig. 2(a)]; therefore, the

TABLE I. Magnetic and electric properties of the devices for the four systems SV-Pt (wafer A and B), SV-Cu, MTJ-Pt, and MTJ-Cu. M_{eff} , R_{wire} , R_{pillar} , GMR, TMR, and RA are the effective magnetization of the free layer, the wire resistance, the pillar resistance, the giant magnetoresistance, the tunnel magnetoresistance, and the resistance-area product, respectively. The last column indicates the section of the paper referring to each system.

	$\mu_0 M_{eff}$ (mT)	R_{wire} (Ω)	R_{pillar} (Ω)	GMR or TMR (%)	RA ($\Omega \cdot \mu\text{m}^2$)	Section
SV-Pt (wafer A)	-172 ± 6	≈ 150	≈ 4	≈ 7		III
SV-Pt (wafer B)	-79 ± 4	$\approx 150\text{--}215$	$\approx 4\text{--}10$	≈ 6		IV A
SV-Cu	-76 ± 24	≈ 128	≈ 4	≈ 4		IV B
MTJ-Pt	$+226 \pm 2$	≈ 103	≈ 1550	≈ 12	≈ 10	IV B
MTJ-Cu	$+107 \pm 5$	≈ 48	≈ 1150	≈ 12	≈ 10	IV B

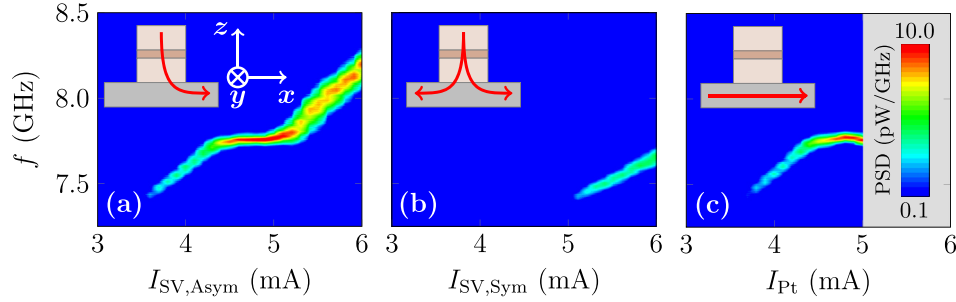


FIG. 2. Two-dimensional plot showing the frequency and power-spectral density (PSD) of the oscillations as a function of the current for a device SV-Pt from sample A. PSD is a logarithmic scale. Measurements are made in the presence of an external field of 250 mT applied at an angle $\theta = 30^\circ$. The device can be excited with SFT and SOT simultaneously (a), with SFT only (b), or with SOT only (c). Figures in insets show cross-sectional diagrams of the current flow (red arrows) through the three-terminal device for each configuration.

STO is excited simultaneously by the SFT and the SOT. The current geometry measured in Fig. 2(a) has the lower critical current, implying that the asymmetric current path induces both SFT and SOT torques. Figure 2(b) describes the excitation of the STO by SFT only. The devices were designed so that when both ends of the Pt layer are grounded [Fig. 2(b)], the current flow is approximately symmetric and nominally no SOTs are generated by electrons flowing in the Pt line, resulting in a higher critical current. Excitation via the Pt line, describing the excitation by SOT only, results in the spectrum shown in Fig. 2(c), which shows a critical current between those seen for $I_{SV,Sym}$ and $I_{SV,Asym}$. We note that the oscillations shown in Fig. 2(c) are measured through the SV without it being explicitly biased. We will see further that the GMR readout is indeed possible due to a small portion of the current shunted through the SV. However, for the description of the method and to consider a simple model, we first make the assumption that no current is shunted through the SV in this configuration, meaning that the STO is entirely excited by the action of the SOT. The limits of this assumption will be discussed in Sec. IV B.

The precession frequency depends on the trajectory of the magnetization precession. Since the same range of precession frequency is obtained with $I_{SV,Sym}$, $I_{SV,Asym}$, and I_{Pt} , we can assume that the three methods excite approximately the same precessional mode in the device. This result shows that the emission spectrum depends mainly on the total spin transfer torque induced by the SOT and/or the SFT, meaning that the inductive fields (that we estimate as less than 5% of the external magnetic field) and the Joule heating induced by the currents through the SV and through the Pt do not have a noticeable effect on the precessional mode at the first order. Therefore, we can use the relative current values to compare the efficiency of each excitation. For the three cases described above, the precession frequency f_{prec} is determined by Lorentzian fits to the spectra, plotted in Fig. 3 as a function of the current (filled symbols). We see that the three curves can be superimposed by simply rescaling the values of the currents I_{Pt} and $I_{SV,Asym}$ of the data in Fig. 2 (open symbols in Fig. 3). The current $I_{SV,Sym}$ is here kept unchanged as a reference. The superposition of the three curves is obtained by determining the best correlation between $f_{prec}(I_{SV,Sym})$ and the curves of $f_{prec}(I_{Pt})$ and $f_{prec}(I_{SV,Asym})$ horizontally scaled in current, which can be described by

$$\begin{aligned} f_{prec}(I_{SV,Sym}) &= f_{prec}\left(I_{Pt} \times \frac{I_{SV,Sym}^0}{I_{Pt}^0}\right) \\ &= f_{prec}\left(I_{SV,Asym} \times \frac{I_{SV,Sym}^0}{I_{SV,Asym}^0}\right), \end{aligned} \quad (1)$$

where I_{Pt}^0 , $I_{SV,Sym}^0$, and $I_{SV,Asym}^0$ are the current values needed to get the same amount τ_0 of angular momentum transfer to the free layer with currents I_{Pt} , $I_{SV,Sym}$, and $I_{SV,Asym}$. This comparison technique is more reliable than simply comparing the onset currents for each excitation because it takes into account all the data points included into the common precession frequency range.

Considering Eq. (1), we find that $I_{SV,Sym}^0/I_{Pt}^0 = I_{SV,Sym}^0/I_{SV,Asym}^0 = 1.4$ for the device shown in Figs. 2 and 3. From the ratio $I_{SV,Sym}^0/I_{Pt}^0$, we see that 1.4 times more current is needed through the SV than through the Pt to get the same oscillations, meaning that the SOT is more efficient in terms of current than the SFT for this device. Moreover, the ratio $I_{SV,Sym}^0/I_{SV,Asym}^0$ shows that 1.4 times more current is needed through the SV with $I_{SV,Sym}$ (excitation by SFT only) than with $I_{SV,Asym}$ (excitation by SFT and SOT) to get similar oscillations, meaning that the part of the current flowing through the Pt wire contributes to 40% of the spin transfer when the current is injected from P3 to P2. Finally, the same results of the ratio $I_{SV,Sym}^0/I_{Pt}^0$

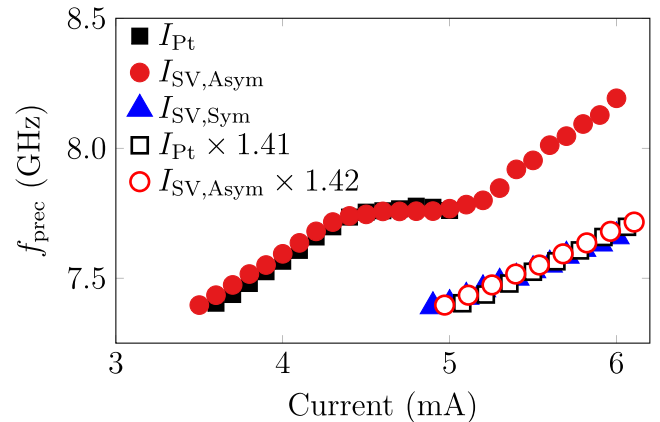


FIG. 3. Precession frequency as a function of the current for the oscillations shown in Figs. 2(a)–2(c) (filled symbols). All the curves can be superimposed by rescaling the current axis of I_{Pt} and $I_{SV,Asym}$ (opened symbols, factors of 1.41 and 1.42). The current axis of $I_{SV,Sym}$ is kept unchanged as a reference. The error bars given by the standard error are smaller than the data points in the plot.

and $I_{SV,Sym}^0/I_{SV,Asym}^0$ (within an error bar of 0.05) are obtained when the field angle is varied between $\theta = 5^\circ$ and $\theta = 35^\circ$.

B. Methodologies for comparison of STT efficiency

We present a methodology to directly compare the efficiencies of exciting oscillations in STOs through SOT and SFT. We define the spin transfer efficiency ε_I in terms of current as the amount τ of spin transfer torque to the free layer per unit current: $\varepsilon_I^{SOT} = \tau/I_{Pt}$ for the SOT and $\varepsilon_I^{SFT} = \tau/I_{SV,Sym}$ for the SFT, which compares the torques generated when current flows only through the Pt wire to when current flows through the SV and then symmetrically through the Pt wire. Similarly, the spin transfer efficiency ε_J in terms of current density is defined as the amount τ of spin transfer torque to the free layer per current density: $\varepsilon_J^{SOT} = \tau/J_{Pt}$ for the SOT and $\varepsilon_J^{SFT} = \tau/J_{SV,Sym}$ for the SFT, where J_{Pt} and $J_{SV,Sym}$ are the current densities through the Pt and the SV (in the symmetric configuration). A rigorous estimation of the spin transfer efficiency is challenging due to the difficulty in estimating the value of τ , which usually relies on an estimation of many parameters (the polarization, the spin-Hall angle, the spin-diffusion length, etc.). However, a comparison of the SOT and the SFT spin transfer efficiency is more straightforward with the three-terminal device because the same amount of spin transfer is needed from both mechanisms to produce an identical excitation.

1. Comparison of efficiencies per unit current

The simplest way to compare the efficiency of SOT and SFT is to compare the amount of current needed to get the same amount of angular momentum transfer τ_0 to the free layer with currents I_{Pt} and $I_{SV,Sym}$. Therefore, the relative spin transfer efficiencies of the SFT and the SOT are obtained by the relative current values of I_{Pt}^0 and $I_{SV,Sym}^0$

$$\frac{\varepsilon_I^{SOT}}{\varepsilon_I^{SFT}} = \frac{I_{SV,Sym}^0}{I_{Pt}^0}. \quad (2)$$

Hence, for the device presented in Fig. 2, the SOT efficiency is 1.4 times the SFT efficiency in terms of current.

For larger widths of the Pt wire (typically for $w_{Pt} \geq 500$ nm), the spin current induced by I_{Pt} with SOT can be too low to induce oscillations because the current density is reduced. In this case, we compare the spin transfer efficiencies with an indirect method by exciting the device with a current $I_{SV,Asym}$ through the SV and perturbing these oscillations by adding a small current I_{Pt} (≤ 1 mA) through the Pt wire [see the inset in Fig. 4(a)]. The efficiency of the SFT and the SOT can then be compared by measuring the influence of the perturbing current I_{Pt} on the oscillations induced by the current $I_{SV,Asym}$. Figure 4(a) shows the precession frequency as a function of $I_{SV,Asym}$ for different values of I_{Pt} measured on the same device as presented in Fig. 2. All the curves have the same shape, and any of them can be superimposed onto the $I_{Pt} = 0$ mA curve by a simple horizontal shift $\Delta I_{SV,Asym}$ of the current value $I_{SV,Asym}$ that depends on the value of I_{Pt} [Fig. 4(b)]. Positive I_{Pt} produces a damping-like torque acting in the same direction as the SFT, resulting

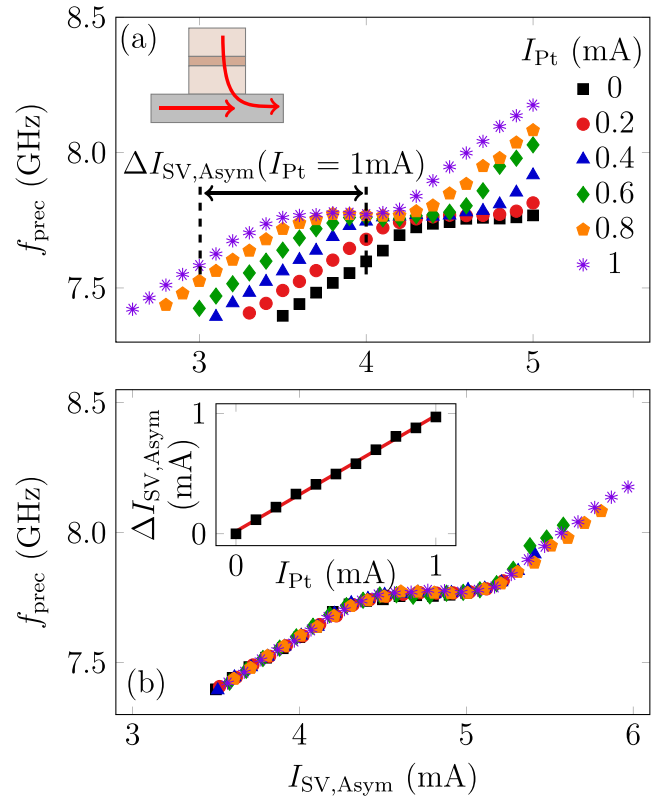


FIG. 4. (a) Precession frequency as a function of current through the SV and through the Pt for the same sample as the one in Fig. 2. The error bars given by the standard error are smaller than the data points. The inset shows a cross-sectional diagram of the current flows (red arrows) through the three-terminal device. (b) All curves can be superimposed using an horizontal translation of $\Delta I_{SV,Asym}(I_{Pt})$. The inset shows the shift $\Delta I_{SV,Asym}$ as a function of the current through the Pt with a linear fit to the data.

in a lower $I_{SV,Asym}$ current needed for the onset of oscillations. In contrary, negative I_{Pt} (not shown here) decreases the total effective spin transfer torque, resulting in a higher current $I_{SV,Asym}$ needed to induce oscillations. The relative spin transfer efficiencies of the SOT and the SFT can then be obtained by

$$\frac{\varepsilon_I^{SOT}}{\varepsilon_I^{SFT}} = \frac{\Delta I_{SV,Asym}(I_{Pt})}{I_{Pt}} \times \frac{I_{SV,Sym}^0}{I_{SV,Asym}^0}. \quad (3)$$

The first ratio on the right corresponds to the amount of current $\Delta I_{SV,Asym}$ needed to compensate for the variation of spin transfer induced by a small amount of current I_{Pt} . This ratio is obtained from a linear fit of $\Delta I_{SV,Asym}$ as a function of I_{Pt} as shown in the inset of Fig. 4(b) and has a value of $\Delta I_{SV,Asym}(I_{Pt})/I_{Pt} = 1.0$ for the device shown. As seen below, this ratio will change based on the Pt wire width. The second ratio in the right term of Eq. (3) corresponds to the rescaling factor needed to correct for the proportion of spin transfer coming from the SOT for a given $I_{SV,Asym}$. From this method, we then obtain $\varepsilon_I^{SOT}/\varepsilon_I^{SFT} = 1.4$, which is consistent with the value obtained from Eq. (2).

2. Comparison of efficiencies per unit current density

While the previous comparison of efficiency per unit current should depend on the dimensions of the device, the

efficiency of the spin transfer in terms of current density is intrinsic to the materials and should be geometry independent. The efficiency per unit current density ε_j is given by the ratio of the efficiency per current unit ε_I over the cross-section area of the current I_{SV} or I_{Pt} . Consequently, the relative efficiencies of the SOT and the SFT per unit current density are given by

$$\frac{\varepsilon_j^{SOT}}{\varepsilon_j^{SFT}} = \frac{\varepsilon_I^{SOT}}{\varepsilon_I^{SFT}} \times \frac{4t_{Pt}w_{Pt}}{\pi L_{SV}w_{SV}}, \quad (4)$$

where t_{Pt} , L_{SV} , and w_{SV} are the Pt thickness, SV length, and SV width, respectively. For the dimensions of the device studied here ($t_{Pt} = 7$ nm, $w_{Pt} = 400$ nm, $L_{SV} = 150$ nm, and $w_{SV} = 50$ nm), we obtain a ratio of $\varepsilon_j^{SOT}/\varepsilon_j^{SFT} = 0.7$. Hence, although more current is required to excite the device with SFT than with SOT for this size of the device, we see that the SFT efficiency is higher than the SOT efficiency in terms of current density.

IV. EXPERIMENTAL RESULTS AND DISCUSSION

A. Comparison of SFT and SOT efficiencies

Using the two methods described above, we compare the SOT and SFT spin transfer efficiencies in terms of current and current density for devices (from wafer B) where the widths of the Pt wires and the SV dimensions are varied. These measurements were made with an external field ranging from 100 mT to 250 mT applied at an angle $\theta = 25^\circ$. Figure 5 shows the ratio $\varepsilon_I^{SOT}/\varepsilon_I^{SFT}$ (black symbols) and $\varepsilon_j^{SOT}/\varepsilon_j^{SFT}$ (red symbols) as a function of the Pt wire width for two different SV dimensions. The error bars are determined experimentally based on the best correlation of $f_{\text{prec}}(I_{SV,\text{Sym}})$ and $f_{\text{res}}(I_{Pt} \times I_{SV,\text{Sym}}/I_{Pt}^0)$ for the values obtained with the direct method [i.e., with Eq. (1)] or based on the standard error of the linear fit of $\Delta I_{SV,\text{Asym}}(I_{Pt})$ and on the best correlation of $f_{\text{prec}}(I_{SV,\text{Sym}})$ and $f_{\text{res}}(I_{Pt} \times I_{SV,\text{Sym}}/I_{SV,\text{Asym}}^0)$ for the values obtained with the indirect method [Eq. (2)]. For the efficiencies in terms of current density, estimated uncertainties of 10 nm for the lithographically defined dimensions (w_{Pt} , L_{SV} , and w_{SV}) and 0.5 nm for the Pt

thickness are included when determining the error bars. This analysis assumes that the spin transfer induced through the SV is entirely due to the SFT mechanism and the spin transfer induced through the Pt wire is entirely due to the SOT mechanism.

Neither ε_j^{SOT} nor ε_j^{SFT} is expected to change with the dimensions of the devices. On the contrary, the spin transfer efficiency in terms of current (ε_I^{SOT} and ε_I^{SFT}) should change with the Pt width and SV size. Experimentally, the ratio of both efficiencies in terms of current density (red symbols) is indeed roughly constant with the Pt width, whereas the ratio $\varepsilon_I^{SOT}/\varepsilon_I^{SFT}$ (black symbols) increases when the Pt width decreases (i.e., for higher current density through the Pt). However, the variation of the SV dimensions does not show the expected behavior. We expect a decrease in the efficiency ε_I^{SFT} when the size of the SV increases and no change in ε_I^{SOT} . However, experimentally, no clear variation of $\varepsilon_I^{SOT}/\varepsilon_I^{SFT}$ occurs with device size, and the ratio $\varepsilon_j^{SOT}/\varepsilon_j^{SFT}$ shows different values for both device sizes. This unexpected result might be due to a difference in the aspect ratio for both sizes of the nanopillar or due to an inaccurate estimation of the dimensions of the nanopillar.

From a quantitative point of view, the efficiencies of both mechanisms are equivalent per unit current for a Pt width close to 700 nm, and the SOT efficiency per unit current can be twice that of the SFT for the narrowest Pt wires. In terms of current density, the SFT efficiency is approximately 1.2 or 3 times higher than the SOT, depending on the size of the device. These numbers can be compared to the literature using the expressions for the damping-like torques for the SOT and the SFT

$$\vec{\tau}_{SFT} = \frac{\gamma \hbar P J_{SV}}{4eM_S t_{FM}} \hat{m} \times (\hat{m} \times \hat{m}_P), \quad (5)$$

$$\vec{\tau}_{SOT} = \frac{\gamma \hbar \theta_{SH} J_{Pt}}{2eM_S t_{FM}} \hat{m} \times (\hat{m} \times \hat{s}), \quad (6)$$

in which P is the spin-current polarization, e is the electron charge, M_S is the saturation magnetization of the free layer, t_{FM} is the thickness of the free layer, θ_{SH} is the spin-Hall angle of the Pt, \hat{m} is the unit vector of the free layer magnetization, \hat{m}_P is the unit vector of the reference layer magnetization, and \hat{s} is the unit vector of the injected spin moment from the Pt into the free layer. Note that Eq. (6) assumes that the damping-like SOT is entirely due to the spin Hall effect. Based on Eqs. (5) and (6) and the knowledge that \hat{m}_P and \hat{s} are identical in this geometry, a comparison of the efficiencies is given by

$$\frac{\varepsilon_I^{SOT}}{\varepsilon_I^{SFT}} = \frac{2\theta_{SH}}{P} \frac{\pi L_{SV} w_{SV}}{4t_{Pt} w_{Pt}} \quad \text{and} \quad \frac{\varepsilon_j^{SOT}}{\varepsilon_j^{SFT}} = \frac{2\theta_{SH}}{P}. \quad (7)$$

Considering the large range of $\theta_{SH} = 1\%$ to 10% in the literature for Pt^{11,12} and a spin-polarization P ranging from 0.3 to 0.6 (generally consistent with transition metal ferromagnets¹³⁻¹⁵), the ratio $\varepsilon_j^{SOT}/\varepsilon_j^{SFT}$ is expected to range between 0.03 and 0.67, which is consistent with the range defined by the error bars shown in Fig. 5.

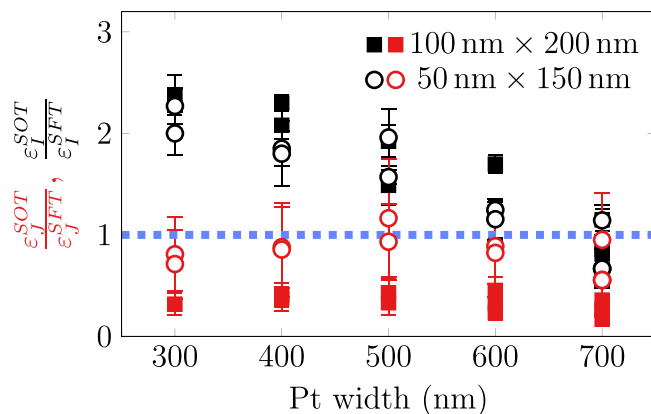


FIG. 5. Comparison of SFT and SOT efficiencies in terms of current (black symbols) and in terms of current density (red symbols) as a function of the Pt width for 22 devices of different dimensions. The error bars are estimated experimentally (see details in the text). The dashed-blue line indicates the equal efficiency of both mechanisms (ratios of unity).

B. Limits of the comparison methods

The comparison above was made under the approximation that no current from I_{Pt} shunts through the SV and that the oscillations excited by I_{Pt} are entirely due to the SOT. However, because the system studied here is metallic (SV with a Cu barrier), it is likely that the current from I_{Pt} is partially shunted through the SV, potentially altering the assumed current density and possibly inducing additional torques. To test the relevance of this approximation, we compare the SV-Pt device with a control sample composed of a SV patterned on a 300 nm wide Cu wire (SV-Cu), for which no SOT is expected. Using the same experimental setup as in Fig. 1, we study the magnetization dynamics when a current I_{Cu} is applied only through the Cu wire, with a magnetic field of 100 mT applied at an angle $\theta = 25^\circ$. Figure 6 shows that, despite the absence of SOT, the current I_{Cu} can also give rise to oscillations of the STO. This result shows the presence of a spin transfer torque whose origin cannot be simply attributed to the standard SOT associated with heavy metals. Therefore, this additional term of spin transfer (that we identify below) must be removed to maintain the validity of the comparison methods presented above.

A potential explanation for the oscillations induced by I_{Cu} is that a portion of the current is shunted into the SV, giving rise to an additional term of SFT. To test this hypothesis, we built two devices consisting of a MTJ on a Pt wire (MTJ-Pt device) and a MTJ on a Cu wire (MTJ-Cu device). In this case, only little current is shunted through both layers of the magnetic stack since they are separated by an insulating barrier. Moreover, since the tunnel barrier is thick, no SFT is expected either. Using the same experimental setup as described in Fig. 1, we study the magnetization dynamics as a function of a current applied through the Pt wire for the MTJ-Pt device [Fig. 7(a)] or through the Cu wire for the MTJ-Cu device [Fig. 7(b)]. In this case, a small current flowing from P1 to P3 ($I_{MTJ,Asym} = 50 \mu A$ for the MTJ-Pt device or $I_{MTJ,Asym} = 200 \mu A$ for the MTJ-Cu device) is applied through the MTJ for the readout of the oscillations through the TMR effect.

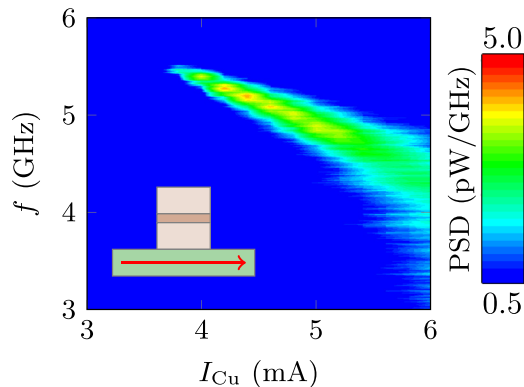


FIG. 6. Two-dimensional plot of the frequency and the PSD (on a logarithmic scale) of a device SV-Cu STO as a function of current I_{Cu} through the Cu wire. The measurement is done in the presence of an external field of 100 mT applied with an angle $\theta = 25^\circ$. The inset shows a cross-sectional diagram of the current flow (red arrow) through the Cu wire in the three-terminal device.

Figure 7(a) shows that, similar to the SV-Pt devices, oscillations can be excited in the MTJ-Pt device with a current I_{Pt} due to the SOT. As expected, the oscillations appear for only one direction of I_{Pt} where the spin transfer torque due to the SOT compensates the damping. The output frequency red shifts with current and increases in amplitude, indicating an increase in the precessional cone angle with current. The same measurement was performed with the MTJ-Cu device, as shown in Fig. 7(b). In this case, a larger current $I_{MTJ,Asym} = 200 \mu A$ through the MTJ is needed to obtain oscillations, and a weak oscillation signal whose amplitude does not depend on the sign or magnitude of the current I_{Cu} is measured, along with a frequency decrease of ≈ 310 MHz from $I_{Cu} = -4$ mA to $I_{Cu} = 4$ mA [Fig. 7(b)]. We attribute this signal to thermally excited ferromagnetic resonance due to the current $I_{MTJ,Asym} = 200 \mu A$ applied through the MTJ. Moreover, we estimate that a variation of current $\Delta I_{Cu} = 8$ mA can induce a change in the Oersted field of $\mu_0 H \approx 10.0$ mT that is expected to induce a frequency shift of ≈ 280 MHz, which is roughly consistent with the frequency change measured experimentally. This result suggests that, unlike the SV-Cu device, no spin transfer is induced by I_{Cu} in the MTJ-Cu device. This supports the conclusion that the oscillations in the SV-Cu device are due to a current shunted through the device. As a consequence, the MTJ-based device is the most appropriate architecture to apply the method presented above because no additional torque other than the SOT induced by I_{Pt} and the SFT induced by $I_{SV,Sym}$ is present in the system. Such a device will need to be fabricated with a lower resistance-area product tunnel barrier than those

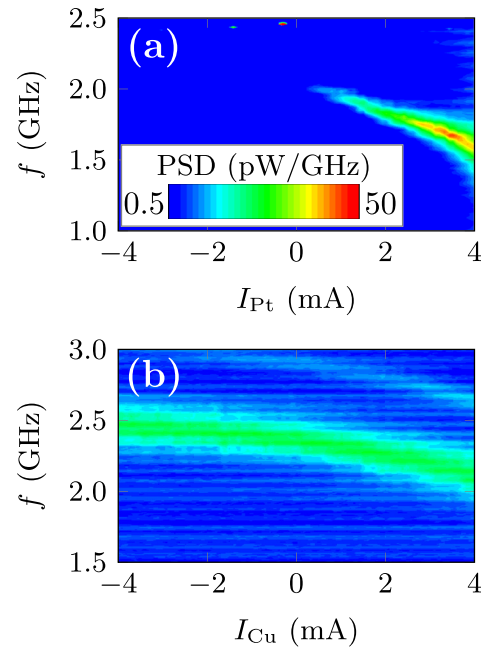


FIG. 7. (a) Two-dimensional plots of the frequency and the PSD (on a logarithmic scale) of a device MTJ-Pt STO as a function of current I_{Pt} through the Pt wire. The measurement is done in the presence of a current $I_{MTJ,Asym} = 50 \mu A$ and an external field of 150 mT applied with an angle $\theta = 10^\circ$. (b) Similar measurement for a device MTJ-Cu STO as a function of current I_{Cu} through the Cu wire. The measurement is done in the presence of a current $I_{MTJ,Asym} = 200 \mu A$ and an external field of 200 mT applied with an angle $\theta = 10^\circ$.

presented here in order to sustain enough DC current through the MTJ to induce the SFT without damaging the tunnel barrier. Alternatively, pulsed switching distributions rather than self-oscillations could be used to compare relative efficiencies.

V. SUMMARY

In summary, we have developed a methodology to directly compare the relative SFT and SOT spin transfer efficiencies in individual three-terminal STOs. Because this method does not require an independent quantification of both torques, the efficiencies of the two mechanisms can be compared in terms of current with no need for parameter estimations, and the efficiencies in terms of current density are compared using only estimations of the device dimensions. Assuming that the spin transfer induced by I_{Pt} is entirely due to the SOT, we show that in this system, the SOT can be more than twice as efficient as the SFT in terms of current for Pt widths of ≈ 300 nm. In terms of current density, the SFT efficiency is up to three times the SOT efficiency. These values are consistent with those of P and θ_{SH} in the literature. Finally, we studied different systems to discuss the limits of the comparison method and showed that a MTJ-based oscillator is the most appropriate device for the application of this method.

ACKNOWLEDGMENTS

This work was partially supported by the DARPA UPSIDE program.

Contribution of the National Institute of Standards and Technology, not subject to copyright in the U.S.

¹A. D. Kent and D. C. Worledge, "A new spin on magnetic memories," *Nat. Nanotechnol.* **10**(3), 187–191 (2015).

- ²S. A. Wolf, "Spintronics: A spin-based electronics vision for the future," *Science* **294**(5546), 1488–1495 (2001).
- ³A. Makarov, T. Windbacher, V. Sverdlov, and S. Selberherr, "CMOS-compatible spintronic devices: A review," *Semicond. Sci. Technol.* **31**(11), 113006 (2016).
- ⁴J. C. Slonczewski, "Current-driven excitation of magnetic multilayers," *J. Magn. Magn. Mater.* **159**(1–2), L1–L7 (1996).
- ⁵L. Berger, "Emission of spin waves by a magnetic multilayer traversed by a current," *Phys. Rev. B* **54**(13), 9353–9358 (1996).
- ⁶I. M. Miron, G. Gaudin, S. Auffret, B. Rodmacq, A. Schuhl, S. Pizzini, J. Vogel, and P. Gambardella, "Current-driven spin torque induced by the Rashba effect in a ferromagnetic metal layer," *Nat. Mater.* **9**(3), 230–234 (2010).
- ⁷I. M. Miron, K. Garello, G. Gaudin, P.-J. Zermatten, M. V. Costache, S. Auffret, S. Bandiera, B. Rodmacq, A. Schuhl, and P. Gambardella, "Perpendicular switching of a single ferromagnetic layer induced by in-plane current injection," *Nature* **476**(7359), 189–193 (2011).
- ⁸L. Q. Liu, C.-F. Pai, Y. Li, H. W. Tseng, D. C. Ralph, and R. A. Buhrman, "Spin-torque switching with the giant spin hall effect of tantalum," *Science* **336**(6081), 555–558 (2012).
- ⁹A. Hoffmann, "Spin hall effects in metals," *IEEE Trans. Magn.* **49**(10), 5172–5193 (2013).
- ¹⁰J. M. Shaw, H. T. Nembach, and T. J. Silva, "Damping phenomena in Co90Fe10/Ni multilayers and alloys," *Appl. Phys. Lett.* **99**(1), 12503 (2011).
- ¹¹J.-C. Rojas-Sánchez, N. Reyren, P. Laczkowski, W. Savero, J.-P. Attané, C. Deranlot, M. Jamet, J.-M. George, L. Vila, and H. Jaffrès, "Spin pumping and inverse spin hall effect in platinum: The essential role of spin-memory loss at metallic interfaces," *Phys. Rev. Lett.* **112**(10), 106602 (2014).
- ¹²W. Zhang, W. Han, X. Jiang, S.-H. Yang, and S. S. P. Parkin, "Role of transparency of platinum–ferromagnet interfaces in determining the intrinsic magnitude of the spin Hall effect," *Nat. Phys.* **11**(6), 496–502 (2015).
- ¹³G. J. Strijkers, Y. Ji, F. Y. Yang, C. L. Chien, and J. M. Byers, "Andreev reflections at metal/superconductor point contacts: Measurement and analysis," *Phys. Rev. B* **63**(10), 104510 (2001).
- ¹⁴W. P. Pratt, S. D. Steenwyk, S. Y. Hsu, W.-C. Chiang, A. C. Schaefer, R. Loloee, and J. Bass, "Perpendicular-current transport in exchange-biased spin-valves," *IEEE Trans. Magn.* **33**(5), 3505–3510 (1997).
- ¹⁵B. Nadgorny, R. J. Soulen, Jr., M. S. Osofsky, I. I. Mazin, G. Laprade, R. J. M. Van De Veerdonk, aa Smits, S. F. Cheng, E. F. Skelton, and S. B. Qadri, "Transport spin polarization of Ni_xFe_{1-x} : Electronic kinematics and band structure," *Phys. Rev. B* **61**(6), R3788–R3791 (1999).